



**Fractal Compression Using Hierarchical Clustered
Peer Adjacent Domain and Multiclass SVM for
Computed Radiography Images**

by

**Norazeani binti Abdul Rahman
(1840312882)**

A report submitted in fulfillment of the requirements for the degree of
Doctor of Philosophy

**Faculty of Electronic Engineering Technology
UNIVERSITI MALAYSIA PERLIS**

2022

ACKNOWLEDGEMENT

Alhamdulillah, segala puji bagi Allah SWT yang telah memberikan ilmu, kekuatan dan kesabaran. Doa saya, Allah SWT sentiasa memberkati ilmu ini dan menjadikan saya hambaNya yang lebih bertakwa.

Setinggi-tinggi penghargaan saya tujukan kepada Penyelia, Prof Ir Dr Rizalafande bin Che Ismail atas segala sokongan dan tunjuk ajar yang diberikan sepanjang kajian ini dijalankan. Kata-kata nasihat dan nilai positif yang Prof tunjukkan akan terus menjadi teladan buat saya.

Dengan hati yang ikhlas, jutaan terima kasih buat suami tercinta, Ahmad Husni bin Mohd Shapri dan anak-anak yang amat dikasihi, Ahmad Raif, Nur Zahra, Ahmad Zarif dan Nur Wafa yang sentiasa setia di sisi memberikan semangat, dorongan dan sokongan serta doa yang berterusan. Pengorbanan yang dicurahkan pastinya akan sentiasa dikenang dan menjadi ingatan berkekalan hingga akhir hayat.

Juga tidak lupa pada Abah dan Mama, Abdul Rahman bin Abu Bakar dan Wan Paziah binti Wan Mohd Amin yang sentiasa mendoakan yang terbaik untuk anak ini. Buat kedua Mertua yang dikasihi, Mohd Shapri bin Husin dan Inson binti Kantan, terima kasih atas dorongan dan doa.

Buat adik-beradik, Abe, Lee, Chik dan Adik, doa serta semangat yang diberikan amatlah Kak hormati. Seterusnya ipar duai, anak-anak saudara dan ahli keluarga yang sentiasa mendoakan, terima kasih atas ingatan kalian. Akhir sekali, terima kasih juga buat rakan-rakan yang membantu secara langsung dan tidak langsung, sokongan dan budi baik anda semua sentiasa saya kenangi dan hormati.

Semoga Allah SWT membalas segala budi baik kalian semua.

TABLE OF CONTENTS

	PAGE
DECLARATION OF THESIS	i
ACKNOWLEDGEMENT	ii
TABLE OF CONTENTS	iii
LIST OF TABLES	vi
LIST OF FIGURES	vii
LIST OF ABBREVIATIONS	xii
LIST OF SYMBOLS	xiv
ABSTRAK	xv
ABSTRACT	xvii
CHAPTER 1 : INTRODUCTION	1
1.1 Introduction	1
1.2 Problem Statement	6
1.3 Research Objective	10
1.4 Research Scope	11
1.5 Thesis Organization	12
CHAPTER 2 : LITERATURE REVIEW	14
2.1 Introduction	14
2.2 Compression in Digital Images	14
2.3 Fractal Compression	22
2.4 Image Partitioning	29

2.5	Domain Pool and Fractal Codebook	31
2.6	K-means Clustering	37
2.7	Support Vector Machine	42
2.8	Accelerating Encoding	45
2.9	Medical Imaging	54
2.10	Review of Fractal Compression in Medical Images	59
2.11	Summary	67
CHAPTER 3 : METHODOLOGY		70
3.1	Introduction	70
3.2	Fractal Encoder and Decoder	70
3.3	Quadtree Partitioning	73
3.4	Peer Adjacent Domain and PCC Classification	75
3.5	K-means Domain Clustering and SVM Mapping	78
3.6	Test Images	82
3.7	Image Quality Indices	86
3.8	Summary	88
CHAPTER 4 : RESULTS AND DISCUSSION		89
4.1	Introduction	89
4.2	Fractal Parameters	89
4.3	Number of Cluster	98
4.4	Encoding Time Reduction	99
4.5	Machine Learning and Clustering	105
	4.5.1 Standard Test Image	105
	4.5.2 Computed Radiography Images	108
4.6	Summary	118

CHAPTER 5 : CONCLUSION AND FUTURE WORK	120
5.1 Conclusion	120
5.2 Recommendation for Future Work	123
REFERENCES	124
LIST OF PUBLICATIONS	140

©This item is protected by original copyright

LIST OF TABLES

		PAGE
Table 2.1	Example of test image Lena with eight isometric operations	25
Table 2.2	Ratios for sample medical image types (Koff and Shulman, 2006)	58
Table 2.3	Salient points and findings of the selected recent methods	67
Table 3.1	TCIA image collections by anatomic region (Clark et al., 2013)	85
Table 4.1	Evaluation results of various Q_{Th} and range size using CR lung images	96
Table 4.2	Performance of proposed peer adjacent domain with PCC method with different quadtree-based FIC methods for standard test image Lena	100
Table 4.3	Average compression results comparing medical images with various pixel dimension using the proposed method	102
Table 4.4	Performance of different quadtree-based FIC methods for standard test image Lena	106
Table 4.5	Performance evaluation of the proposed method executed using SMPTE test pattern with various pixel dimensions of different range sizes	107
Table 4.6	Average values of proposed method evaluation executed using 360 CR images (2048×2048) with and without chest lung nodules for different range sizes and $Q_{Th} 0.2$	109

LIST OF FIGURES

	PAGE	
Figure 1.1	The basic flow of image compression technique	5
Figure 2.1	Lossy compression scheme	18
Figure 2.2	Example of self-similarity in test image Lena	23
Figure 2.3	Block diagram of fractal image compression	29
Figure 2.4	Example of quadtree partitioning	30
Figure 2.5	Example of quadtree partitioning of a range with four iterations	31
Figure 2.6	Spiral search approach (Barthel and Voyé, 1994)	34
Figure 2.7	The K-means clustering algorithm procedure	41
Figure 2.8	Separation of two data classes via an optimal hyperplane in SVM (Cardoso-Fernandes et al., 2020)	43
Figure 2.9	Example of (a) linear and (b) non-linear hyperplane in SVM (Nisbet et al., 2009)	44
Figure 3.1	Flow chart of the conventional FIC algorithm	71
Figure 3.2	Flow chart of the proposed encoding FIC algorithm	72
Figure 3.3	Concept of quadtree partitioning	74
Figure 3.4	Example of quadtree partitioning using test image Lena	74
Figure 3.5	Peer adjacent domain in each hierarchy	75
Figure 3.6	Peer adjacent domain method	76

Figure 3.7	Example of peer adjacent domain in each hierarchy; (a,b) range size 8×8 and adjacent domain size 16×16 , (c,d) range size 4×4 and adjacent domain size 8×8 , (e,f) range size 2×2 and adjacent domain size 4×4	77
Figure 3.8	SVM mapping in hierarchical layer	80
Figure 3.9	Example of N layers of K-means clustering and unsupervised multiclass SVM mapping	81
Figure 3.10	Standard test image Lena in greyscale	82
Figure 3.11	SMPTE RP-133 medical diagnostic imaging test pattern (Enstrom et al., 2000)	83
Figure 3.12	Sample of (a) MRI, (b) CT, and (c) mammography images from TCIA (Clark et al., 2013) and (d) CR image from JSRT (Shiraishi et al., 2000)	86
Figure 4.1	Evaluation results of (a) PSNR and (b) C_{ratio} and encoding time for various Q_{Th} values using the SMPTE test image	90
Figure 4.2	Compression results for various Q_{Th} values using the SMPTE test image, (a) Q_{Th} 0, (b) Q_{Th} 0.1, (c) Q_{Th} 0.2, (d) Q_{Th} 0.3, (e) Q_{Th} 0.4 and (f) Q_{Th} 0.5	91
Figure 4.3	Evaluation results of (a) PSNR and (b) C_{ratio} and encoding time for various range sizes using the SMPTE test image	92
Figure 4.4	Compression image results for various range sizes using the SMPTE test image, (a) range size (1,2), (b) range size (2,4), (c) range size (4,8), (d) range size (8,16), (e) range size (16,32) and (f) range size (32,64)	93
Figure 4.5	Evaluation results of (a) PSNR and (b) decoding time for a various number of iterations at the fractal decoder using the SMPTE test image	94

Figure 4.6	Compression image results for various number of iterations at the fractal decoder using the SMPTE test image, (a) 1 iteration, (b) 2 iterations, (c) 3 iterations, (d) 4 iterations, (e) 5 iterations and (f) 6 iterations.	95
Figure 4.7	Sample of the reconstructed image of the proposed method, (a) a ground truth 2048×2048 CR lung test image, (b-d) compressed image with range size (2,4) $Q_{Th} 0$, range size (2,4) $Q_{Th} 0.2$, and range size (4,8) $Q_{Th} 0.2$, respectively	97
Figure 4.8	Optimum number of clusters using the silhouette method	99
Figure 4.9	Compression result of test image Lena, (a) original image, (b) Wang and Zhang (c) Xing-Yuan et al. (d) Gupta et al. and (e) proposed method	101
Figure 4.10	Sample of compression result of selected MRI images (pixel dimension of 256×256) using the proposed method. (a) and (c) are the original image (uncompressed) and compressed image at range (2,4). (b) and (d) are the closed-up view of each original and compressed image	103
Figure 4.11	Sample of compression result of selected CT images pixel dimension of 512×512) using the proposed method. (a) and (c) are the original image (uncompressed) and compressed image at range (2,4). (b) and (d) are the closed-up view of each original and compressed image	104
Figure 4.12	Sample of compression result of selected CR images (pixel dimension of 2048×2048) using the proposed method. (a) and (c) are the original image (uncompressed) and compressed image at range (4,8). (b) and (d) are the closed-up view of each original and compressed image	104
Figure 4.13	Sample of compression result of selected mammography images (pixel dimension of 4096×4096) using the proposed	

	method. (a) and (c) are the original image (uncompressed) and compressed image at range (8,16). (b) and (d) are the closed-up view of each original and compressed image	104
Figure 4.14	Compression result of test image Lena, (a) original image, (b) Wang and Zhang (c) Xing-Yuan et al. (d) Gupta et al. and (e) proposed method	106
Figure 4.15	Sample of compression result of selected CR images (with nodule) using proposed method. (a) original image (uncompressed), (b) compressed at range (2,4), PSNR = 47.32 dB, $C_{ratio} = 5.70$, (c) compressed at range (4,8), PSNR = 39.63 dB, $C_{ratio} = 23.56$, (d) compressed at range (8,16), PSNR = 37.32 dB, $C_{ratio} = 73.98$, (e-h) closed-up view of nodule (mark as small box) of each original and compressed image	112
Figure 4.16	Sample of compression result of selected CR images (with nodule) using proposed method. (a) original image (uncompressed), (b) compressed at range (2,4), PSNR = 45.65 dB, $C_{ratio} = 6.12$, (c) compressed at range (4,8), PSNR = 40.70 dB, $C_{ratio} = 22.95$, (d) compressed at range (8,16), PSNR = 38.01 dB, $C_{ratio} = 73.53$, (e-h) closed-up view of nodule (mark as small box) of each original and compressed image	113
Figure 4.17	Sample of compression result of selected CR images (with nodule) using proposed method. (a) original image (uncompressed), (b) compressed at range (2,4), PSNR = 45.98 dB, $C_{ratio} = 5.98$, (c) compressed at range (4,8), PSNR = 41.52 dB, $C_{ratio} = 22.13$, (d) compressed at range (8,16), PSNR = 39.82 dB, $C_{ratio} = 71.22$, (e-h) closed-up view of nodule (mark as small box) of each original and compressed image	114
Figure 4.18	Sample of compression result of selected CR images (with nodule) using proposed method. (a) original image (uncompressed), (b) compressed at range (2,4), PSNR = 45.70 dB, $C_{ratio} = 5.99$, (c) compressed at range (4,8), PSNR = 39.95	

dB, $C_{ratio} = 23.24$, (d) compressed at range (8,16), PSNR = 37.86 dB, $C_{ratio} = 73.66$, (e-h) closed-up view of nodule (mark as small box) of each original and compressed image 115

Figure 4.19 Sample of compression result of selected CR images (with nodule) using proposed method. (a) original image (uncompressed), (b) compressed at range (2,4), PSNR = 46.69 dB, $C_{ratio} = 5.74$, (c) compressed at range (4,8), PSNR = 40.95 dB, $C_{ratio} = 22.87$, (d) compressed at range (8,16), PSNR = 38.69 dB, $C_{ratio} = 72.21$, (e-h) closed-up view of nodule (mark as small box) of each original and compressed image 116

Figure 4.20 Sample of compression result of selected CR images (with nodule) using proposed method. (a) original image (uncompressed), (b) compressed at range (2,4), PSNR = 45.30 dB, $C_{ratio} = 6.15$, (c) compressed at range (4,8), PSNR = 41.64 dB, $C_{ratio} = 22.04$, (d) compressed at range (8,16), PSNR = 37.68 dB, $C_{ratio} = 73.80$, (e-h) closed-up view of nodule (mark as small box) of each original and compressed image 117

LIST OF ABBREVIATIONS

18F PET-CT	18F-fluorodeoxyglucose PET-CT
2D	two-dimensional
3D	three-dimensional
ANN	artificial neural network
BPG	better portable graphics
BWT	Burrows–Wheeler transform
CAT	computerized axial tomography
CR	computed radiography
CT	computed tomography
CTP	computed tomography perfusion
DCT	discrete cosine transform
DF	digital fluoroscopy
DICOM	digital imaging and communications in medicine
DM	digital mammography
DR	digital radiography
DWT	discrete wavelet transform
EZW	embedded zero-tree wavelet
FD	fractal dimension
FFT	fast Fourier transform
FIC	fractal image compression
fMRI	functional magnetic resonance imaging
IFS	iterated function system
JPEG	Joint Photographic Experts Group
JPEG-LS	Joint Photographic Experts Group-Lossless Standard
JSRT	Japanese Society of Radiological Technology
K-NN	k-nearest neighbour
KLT	Karhunen-Loève transforms
LEZW	lossless embedded zerotree wavelet encoder
LZW	Lempel–Ziv–Welch
MRI	magnetic resonance imaging
MTF	move to front transform
NMR	nuclear magnetic resonance
PACS	picture archiving and communication systems

PAM	partitioning around medoids
PCC	Pearson correlation coefficient
PET	positron emission tomography
PIFS	partitioned iterated function system
PNG	portable network graphics
PSNR	peak signal-to-noise ratio
PSO	particle swarm optimization
PSPs	photostimulable phosphors
RDCT	reversible discrete cosine transform
RMSE	root-mean-square error
ROI	region of interest
SMPTE	Society of Motion Picture and Television Engineers
SPIHT	set partitioning in hierarchical trees
SVM	support vector machine
TCIA	The Cancer Imaging Archive
VOI	volume of interest
VQ	vector quantization
WCSS	within-cluster sums of squares

©This item is protected by original copyright

LIST OF SYMBOLS

bs	base
d	distance
D	domain block
F	maximum fluctuation
I	image
\hat{I}	reconstructed image
k	number of clusters
m	centroid
μ	mean
n	number of samples
N	block size
o	offset to the pixel luminance (brightness)
p	probability
Q	scalar observations
R	range block
s	pixel luminance (contrast)
S	silhouette value
σ	standard deviation
ω	contractive affine transformation
W	Hutchinson's operator
x	sample or objects to be cluster
z	pixel's intensity value

Pemampatan Fraktal Menggunakan Domain Rakan Bersebelahan Bergugusan Hierarki dan SVM Multikelas untuk Imej Radiografi Berkomputer

ABSTRAK

Jumlah data dari pengimejan perubatan semakin meningkat dan menggunakan kos penyimpanan data digital yang tinggi. Kaedah yang dapat mengurangkan saiz imej, mengambil-semula imej dengan pantas dan mengekalkan butiran perubatan yang signifikan merupakan suatu penekanan dalam penyelidikan. Oleh itu, pemampatan imej fraktal (FIC) sangat perlu untuk memperoleh nisbah mampatan (C_{ratio}) yang jauh lebih tinggi tanpa kemerosotan imej yang ketara yang mana secara klinikal adalah penting untuk prestasi diagnostik yang berkesan. Fasa pengekodan dalam FIC carian penuh memerlukan masa yang intensif kerana carian berurutan mesti dilaksanakan melalui kumpulan domain besar untuk mencari domain yang paling sesuai bagi setiap blok rentang. Dalam kajian ini, suatu kaedah penambahbaikan untuk FIC berdasarkan domain rakan bersebelahan bergugusan hierarki dan pemetaan mesin vektor sokongan multikelas (SVM) yang tidak diselia bagi imej radiografi berkomputer (CR) telah dicadangkan. Dengan menggunakan pendekatan ini, parameter-parameter fraktal optimum telah dicadangkan untuk meningkatkan kecekapan pengekodan FIC. Kombinasi domain rakan bersebelahan dengan pekali korelasi Pearson (PCC) direkabentuk untuk mengurangkan kerumitan komputasi pengekodan. Domain rakan bersebelahan mempunyai kurang pengiraan memandangkan ianya mengurangkan bilangan blok-blok domain dalam kumpulan domain. PCC digunakan untuk klasifikasi blok domain berdasarkan nilai korelasi, seterusnya mempercepatkan pengekodan. SVM multikelas yang tidak diselia dan penggugusan K-means dikembangkan dalam kajian ini untuk meningkatkan proses pemetaan. Kebaharuan dari pendekatan yang dicadangkan terletak pada penggunaan domain rakan bersebelahan bergugusan hierarki dengan SVM multikelas untuk pemetaan rentang-domain yang tepat, menghasilkan nisbah mampatan yang tinggi dengan penyimpanan yang berkurangan, masa pengambilan-semula yang pantas dan imej bina-semula yang berkualiti tinggi. Kaedah yang dicadangkan telah diuji dengan menggunakan pelbagai imej ujian piawai dan dua set pangkalan data imej perubatan dari *The Cancer Imaging Archive (TCIA)* dan *Japanese Society of Radiological Technology (JSRT)*. Prestasi parameter-parameter fraktal optimum yang dicadangkan dinilai dengan menggunakan imej *Society of Motion Picture and Television Engineers (SMPTE)* dan imej paru-paru radiografi berkomputer. Hasil kajian menunjukkan bahawa parameter fraktal yang optimum adalah saiz rentang bersamaan 4 (minima) dan 8 (maksima), ambang *Quadtree* (Q_{Th}) bersamaan 0.2 dan tiga iterasi penyahkodan. Kaedah yang dicadangkan menunjukkan prestasi yang baik dalam penilaian pengurangan masa pengekodan untuk imej ujian piawai dari segi nisbah isyarat-hingar puncak (PSNR), masa mampatan, dan nisbah mampatan, masing-masing mendapat skor 27.27 dB, 6.88 s dan 16.13. Penilaian terhadap pelbagai modaliti dan saiz imej perubatan daripada *TCIA* menunjukkan bahawa kaedah yang dicadangkan dapat memampatkan imej bersaiz besar dengan lebih baik berbanding imej bersaiz kecil. Untuk 16.3 MB imej mamografi dengan saiz piksel 4096×4096 , kaedah yang dicadangkan mampu mengembalikan imej mampatan kurang daripada satu minit dengan 39.5 dB. Pelaksanaan SVM multikelas dan

penggugusan K-means telah meningkatkan lagi kualiti imej yang dimampatkan. Hasil keputusan untuk penilaian kaedah yang dicadangkan telah dilaksanakan menggunakan 360 imej CR dengan dan tanpa nodul paru-paru dada menunjukkan kualiti imej bina-semula dengan PSNR bersamaan 41 dB untuk saiz rentang (4,8) dan dikodkan kurang dari satu minit. Kaedah yang dicadangkan menjimatkan storan kira-kira 95.6 peratus dengan saiz yang disimpan hanya 358 kB daripada 8193 kB saiz imej asal. Hasil kajian menunjukkan bahawa kaedah yang dicadangkan dapat memperoleh imej bina-semula yang berkualiti dengan penjimatan saiz storan yang lebih besar dan masa pengekodan yang munasabah.

©This item is protected by original copyright

Fractal Compression Using Hierarchical Clustered Peer Adjacent Domain and Multiclass SVM for Computed Radiography Images

ABSTRACT

The volume of data from medical imaging is growing and consumes high costs of digital data storage. A method that can reduce the image size, fast retrieving and preserving the critical medical details of the image is a highlight in the research. Therefore, fractal image compression (FIC) is essential to obtain a substantially higher compression ratio (C_{ratio}) without perceptible image degradation, which is clinically essential for effective diagnostic performance. The encoding phase in full-search FIC is time-intensive as a sequential search must be performed through a massive domain pool to find the best-matched domain for each block of ranges. This study proposes an improved FIC method based on hierarchical clustered peer adjacent domain and unsupervised multiclass support vector machine (SVM) mapping for computed radiography (CR). The optimal fractal parameters were proposed to increase FIC encoding efficiency using this approach. Combining the peer adjacent domain with the Pearson correlation coefficient (PCC) is designed to reduce computational complexity encoding. The peer adjacent domain has fewer computations, reducing the number of domain blocks in a domain pool. The PCC being used for domain block classification based on correlation value speeds up the encoding. The unsupervised multiclass SVM and K-means clustering are developed in the study to improve the mapping process. The novelty of the proposed approach lies in the use of hierarchical clustered peer adjacent domains with multiclass SVM for accurate domain-range mapping, resulting in a high compression ratio with reduced storage, fast retrieving time, and high reconstructed image quality. The proposed method was tested using various standard test images and two sets database of medical images from The Cancer Imaging Archive (TCIA) and the Japanese Society of Radiological Technology (JSRT). The performance of the proposed optimal fractal parameters is evaluated using the Society of Motion Picture and Television Engineers (SMPTE) image and computed radiography lung images. The results show that the optimal fractal parameters for increasing encoding efficiency are quadtree threshold (Q_{Th}) equal to 0.2, range size is (4,8), and three decoding iterations. The proposed method shows good performance in the encoding time reduction evaluation for the standard test image in terms of peak signal-to-noise ratio (PSNR), compression time, and compression ratio, with 27.27 dB, 6.88 s, and 16.13, respectively. Evaluation of various medical image modalities and sizes from TCIA images demonstrates that the proposed method can compress larger images better than small images. For the 16.3 MB 4096×4096 mammography image, the proposed method retrieves the compressed image less than a minute with 39.5 dB. The implementation of multiclass SVM and K-means clustering has further improved the compressed image quality. The results for the proposed method evaluation executed using 360 CR images with and without chest lung nodules showed the high quality of reconstructed images with a PSNR equal to 41 dB for a range size of (4,8) and encoded less than a minute. The proposed method saved the storage about 95.6 percent with stored only 358 kB out of 8193 kB original size image. The finding

demonstrates that the proposed method obtained high quality reconstructed images with more extensive storage and adequate encoding time.

©This item is protected by original copyright

CHAPTER 1 : INTRODUCTION

1.1 Introduction

Nowadays, most of the data is recorded in digital format and almost all image interpretation and analysis involve digital processing. Disciplines, such as medicine, e-commerce, and multimedia, are limited by the interchange of digital images. Online broadcasting in sports events, teleconference at a worldwide company, and even surgery with remote participation from one or more experts, are examples of the use of digital image-related technologies today.

Medical imaging is used to acquire body parts images for medical reasons to detect or investigate illnesses. Every week, millions of imaging operations run globally. The improvements in image processing methods include image recognition, analysis, and enhancement, driving the development of medical imaging. Digitized medical images, such as x-rays, computed tomography (CT), nuclear magnetic resonance (NMR), and ultrasound, include a large number of pixels with about similar brightness, many of which create zones of near homogeneity (Loew and Li, 1994). In the process of diagnosing and treating disease and injury using advanced imaging devices, medical radiologists frequently have to deal with big image data acquired from the patient during a routine medical examination (Kharat and Singhal, 2017).

Every year, billions of images are taken throughout the world for various medical purposes. Approximately half of them utilize ionizing and nonionizing radiation modulators (Abdallah, 2015). Medical imaging generates an image of the body's inner structure without the need for invasive therapies. These images were made using fast processors because of the mathematical and logical translation of energy to signals (Abdallah, 2018). After that, the impulses are translated into digital images. These signals represent the different kinds of tissues found throughout the body.

Therefore, one of the recurring challenges experienced by radiologists is preserving and archiving the images, particularly in situations where they are routinely obtained at the most outstanding possible quality (Varma, 2012). The expanding volume of medical imaging data, especially time series such as CT perfusion (CTP), needs unique and rapid procedures to deliver early results for acute treatment. CTP datasets may currently be as large as 3.76 GB, and when dealing with such a massive quantity of data, traditional data storage techniques are sluggish, inefficient, and even costly in terms of the price of purchasing and maintaining specialized image processing software and hardware (Barros et al., 2016).

Digital acquisition technologies, such as multi-slice CT and digital mammography, may create vast amounts of digital images, subsequently sent to image archiving and communication systems (PACS). PACS and teleradiology technology have posed issues in storing and sending enormous amounts of digital images. These technologies have resulted in an exponential increase of digital image files (Huang, 2019; Pooley, 2001). The number of images taken in a multi-slice CT examination, for example, may range from 40 to 3000. One examination may yield 20 MB or more of data if the

image size is 512×512 . Computed radiography (CR) examination consisting of two images per examination with an image size of 2048×2048 delivers 16 MB of data. A digital mammography exam may presently provide up to 160 MB of data (Huang, 2019). In other words, one of the most significant difficulties of using medical images is their larger size, which makes them challenging to store and transmit. Consequently, image compression, which may reduce image size while retaining image quality, becomes a priority in this study.

The development of coding utilizing entropy by Shannon–Fano started in the 1940s (Kia et al., 1998), which served as the foundation for Huffman coding, introduced in 1950 (Klein et al., 2019). The fast Fourier transform (FFT) introduced transform coding in the late 1960s and the Hadamard transform started early 1969 (Shruthi et al., 2016). The discrete cosine transforms (DCT) produced using fundamental image reduction algorithm was invented in the early 1970s (Kekre and Kulkarni, 2011). DCT compression is the cornerstone of JPEG, introduced in 1992 by the Joint Photographic Experts Group (JPEG). JPEG is the most often used image file format as it compresses images to drastically reduced file sizes. The efficient DCT compression technology was mainly blamed for the widespread acceptance of digital images and digital photographs (Aguilera, 2006).

Meanwhile, the Lempel–Ziv–Welch (LZW) algorithm was devised in 1984. It is employed in the 1987 GIF format (Lowe and Bennett, 2009). The portable network graphics (PNG) format exploits lossless compression method, DEFLATE developed in 1996 (Hosseini, 2012). Wavelets were initially exploited in image compression with the advent of DCT coding (Hoffman, 2012). In the year 2000, the JPEG 2000 standard was

released (Rabbani, 2002). JPEG 2000 employs discrete wavelet transform (DWT) methods instead of the DCT approach utilised by the original JPEG format (Unser and Blu, 2003). In 2004, JPEG 2000 technology was accepted as the digital cinema video coding standard including the Motion JPEG 2000 extension (Swartz, 2004). More research efforts evolved, resulting in enhanced image quality and digital coding (Subramanya, 2001).

The fact that neighbouring pixels are connected and carry duplicate information is a common feature of most images. Image compression's major goal is to minimise image data storage space while also enhancing image transmission speed for huge volumes of digital data, reducing transmission time (Huang, 2019; Ringl et al., 2007; Koff and Shulman, 2006; Seeram, 2005). It must represent an image by reducing as much abstraction and spectral redundancy as possible while preserving the resolution and visual quality of the reconstructed image as close to the original image as possible by leveraging those redundancies. To generate the reconstructed image, an associated inverse procedure known as decompression or decoding is used to the compressed knowledge (Kodgule and Sonkamble, 2015).

According to Singh et al. (2016), the primary goal of image compression algorithms is to reduce the irrelevance or redundancy of an image to offer a facility for effectively storing and conveying data. The first stage in this approach is to change the image from its spatial domain representation into a distinct kind of representation using a few well-known conversions, and then encode the converted quantities such as coefficients. This approach provides the great compression of data as compared to the predictive techniques, however at the expense of the high processing demands. Primarily,

compression is accomplished by reducing any of one or more of three primary data redundancies which are coding redundancy, inter-pixel redundancy and psycho-visual redundancy. Image compression attains redundancy for more efficient coding. Figure 1.1 demonstrates the fundamental flow of image compression technology.

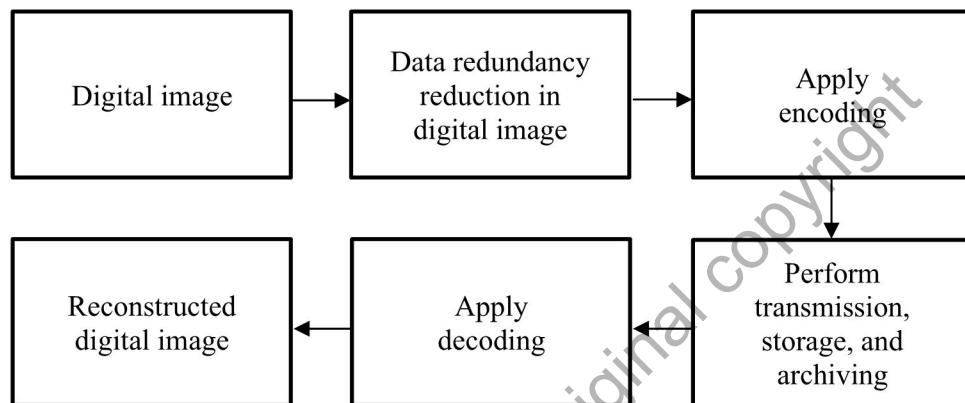


Figure 1.1 The basic flow of image compression technique

Hence, compression is crucial for handling massive medical image collections. This technology enables the image size to be reduced significantly while keeping an appropriate level of signal-to-noise ratio, which is clinically critical for successful diagnostic performance (Smutek, 2005). Highly correlated images such as CR images might have extremely high compression efficiency since most image patches focus on a small number of coefficients when translated into the spatial frequency domain. The less significant coefficients of the converted image may be quantized, resulting in a huge reduction of file size reductions and minimum loss of crucial information. According to Sung et al. (2002), reaching a compression ratio of 10:1 or even higher without compromising diagnostic quality is plausible. In this context, the lossy compression-based fractals favour computer scientists and medical engineers since this technology gives a high compression ratio with less decoding time.

1.2 Problem Statement

Long-lasting storage of any data type may be beneficial. Most hospitals currently depend on the technology of medical imaging for patient care management, which combines an enormous number of medical test findings. Unfortunately, these hospital databases are expanding. Daily, tons of images are made and are usually saved for some time. In truth, medical operations are digital; sophisticated imaging scanning technology and the relevance of volumetric image data sets, contribute to more significant expenditures for more extended image storage needs.

Image resolutions of 512×512 are currently considered the minimal requirement. Modern scanning technologies, on the other hand, may create images 1024×1024 or larger (Huang, 2019). Additionally, the scanning technologies are capable of boosting the amount of output data. The number of slices in volumetric datasets increased when the inter-slice spacing fell from 5 mm to 0.6 mm using thin-slice CT scanning (Goldman, 2008; Riedel et al., 2012). Thus, an effective compression technique enhancing the transmission for processing medical images is of the utmost requirement. Moreover, the internet usage for telemedicine and e-health platforms today demands extensive support for aspects such as region-of-interest coding and progressive quality and resolution scaling more than ever before. Both parts of storage and sharing involving digital data are related to limits that impede the expansion of their uses and the invention of new technologies. When sending image data, one aims to keep high quality; the time necessary for transmission and disk space is needed for storage as low as feasible. However, increases in the throughput utilised in communication are inadequate, and additional solution methods are required to suit the expanding expectations and demands.